IAEA nuclear fusion

LETTER

The interaction between fishbone modes and shear Alfvén waves in tokamak plasmas

IOP Publishing | International Atomic Energy Agency Nuclear Fusion
Nucl. Fusion **56** (2016) 054003 (6pp) doi:10.1088/0029-5515/56/5/054003

Letter

The interaction between fishbone modes and shear Alfvén waves in tokamak plasmas

Hongda He[1], Yueqiang Liu[2,1], J.Q. Dong[1], G.Z. Hao[1], Tingting Wu[3], Zhixiong He[1] and K. Zhao[4]

[1] Southwestern Institute of Physics, Chengdu, People's Republic of China
[2] CCFE, Culham Science Centre, Abingdon, OX14 3DB, UK
[3] Dalian University of Technology, Dalian, People's Republic of China
[4] Southwest University for Nationalities, Chengdu, People's Republic of China

E-mail: hehda@163.com

Received 29 December 2015, revised 19 February 2016
Accepted for publication 1 March 2016
Published 31 March 2016

Abstract

The resonant interaction between the energetic particle triggered fishbone mode and the shear Alfvén waves is computationally investigated and firmly demonstrated based on a tokamak plasma equilibrium, using the self-consistent MHD-kinetic hybrid code MARS-K (Liu *et al* 2008 *Phys. Plasmas* **15** 112503). This type of continuum resonance, occurring critically due to the mode's toroidal rotation in the plasma frame, significantly modifies the eigenmode structure of the fishbone instability, by introducing two large peaks of the perturbed parallel current density near but offside the $q = 1$ rational surface (q is the safety factor). The self-consistently computed radial plasma displacement substantially differs from that being assumed in the conventional fishbone theory.

Keywords: interaction, fishbone mode, shear Alfvén wave

(Some figures may appear in colour only in the online journal)

It is well known that a magnetohydrodynamic (MHD) mode, which is rotating in the plasma frame in a tokamak, can experience resonances with continuum waves such as the shear Alfvén waves and the sound waves. Such types of resonant interactions do not often occur, since many MHD modes, such as the internal kink mode, the tearing mode, the peeling-ballooning mode, the infernal mode, normally rotate together with the plasma, and thus appear static in the plasma frame. One well known exception is the resistive wall mode (RWM), which is an external kink instability, strongly interacting with the surrounding resistive wall(s) in toroidal devices such as tokamaks or reversed field pinches. As a result, the mode is well locked to the wall even when the plasma is rotating. The resonant interaction between the RWM and the continuum waves in a rotating plasma provides one of the key damping mechanisms for the former [1, 2].

In this work, we investigate the similar resonant interaction physics for the internal kink mode, which is driven unstable by kinetic resonances with precessional drift motions of trapped energetic particles (EPs), resulting in the so-called fishbone instability [3]. In other words, the internal kink is stable without the EPs drive. More importantly, the triggered fishbone mode has a finite real frequency even for a static plasma equilibrium, meaning that the mode rotates in the plasma frame. Consequently, the mode experiences resonances with plasma continuum waves, as has already been shown in theory [4]. More specifically, coupling of the fishbone to the shear Alfvén waves is numerically identified, whilst no significant resonance effect from the sound waves is found for the plasma considered in this work.

The key physics consequence, that can be identified from the self-consistent toroidal computations, is the significant modification of the fishbone eigenmode structure near the mode resonant surface. More specifically, two large peaks, for the perturbed parallel current density, appear near but offside the $q = 1$ rational surface. The gap between these two current peaks increases nearly linearly with the fishbone frequency. This is quantitatively confirmed by both toroidal computations and by the analytic estimate. The computed radial displacement of the mode switches sign near the $q = 1$ surface, being qualitatively different from the conventional theory assumptions, of being either a step-like function, or a hyperbolic tangent function describing the smooth transition within the inertial layer.

The aforementioned toroidal computations are performed with the MHD-kinetic hybrid code MARS-K [5]. The code is well benchmarked against other codes with similar drift kinetic effects [6, 7], and has been extensively applied to study MHD perturbations associated with external kink modes [8–11]. One key feature, which allows us to perform the study reported in this work, is the non-perturbative approach employed in the MARS-K formulation. The MHD equations and the drift kinetic equations are solved together in MARS-K, thus allowing (i) the self-consistent modification of the internal kink eigenfunction by the drift kinetic effects from trapped EPs, and (ii) the wave–wave resonance interactions between the fishbone and the plasma continua. Therefore, both types of resonance physics—the resonance between internal kink and EPs and the resonance between fishbone and Alfvén waves, being of different physics origins, are included into the MARS-K model and employed in this study. We also mention that similar self-consistent MHD-kinetic hybrid formulations have been employed in other studies [12–15].

Assuming an ideal plasma with toroidal equilibrium flow, the core equations of the MARS-K model can be written as

$$\mathrm{i}(\omega + n\Omega)\vec{\xi} = \vec{v} + (\vec{\xi} \bullet \nabla\Omega)R^2\nabla\phi, \tag{1}$$

$$\begin{aligned}\mathrm{i}\rho(\omega + n\Omega)\vec{v} = &-\nabla \bullet \vec{p} + \vec{j} \times \vec{B} + \vec{J} \times \vec{Q} \\ &- \rho[2\Omega\widehat{\vec{Z}} \times \vec{v} + (\vec{v} \bullet \nabla\Omega)R^2\nabla\phi],\end{aligned} \tag{2}$$

$$\mathrm{i}(\omega + n\Omega)\vec{Q} = \nabla \times (\vec{v} \times \vec{B}) + (\vec{Q} \bullet \nabla\Omega)R^2\nabla\phi, \tag{3}$$

$$\vec{p} = p_{\parallel}\widehat{\vec{b}}\widehat{\vec{b}} + p_{\perp}(\vec{I} - \widehat{\vec{b}}\widehat{\vec{b}}), \tag{4}$$

$$\vec{j} = \nabla \times \vec{Q}, \tag{5}$$

where variables $\vec{\xi}$, $\vec{v}$, $\vec{Q}$, $\vec{j}$, $\vec{p}$ represent the plasma displacement, the perturbed velocity, magnetic field, current and pressure tensor. ω is the complex eigen-frequency of the mode, defined in the laboratory frame and is subject to a Doppler shift $n\Omega$, with n being the toroidal mode number, Ω the plasma rotation frequency along the toroidal angle ϕ. ρ is the plasma mass density. Variables $\vec{J}$, $\vec{B}$ represent the equilibrium current and magnetic field strength, respectively. R is the major radius. $\widehat{\vec{Z}}$ and $\vec{I}$ are the unit vector in the vertical direction and for the vector tensor, respectively. The kinetic effects are included via the parallel and perpendicular pressure components, evaluated from the perturbed distribution function f_{L}^1

$$p_{\parallel}\mathrm{e}^{-\mathrm{i}\omega t + \mathrm{i}n\phi} = \sum_{\sigma}\int \mathrm{d}\Gamma M v_{\parallel}^2 f_{\mathrm{L}}^1, \tag{6}$$

$$p_{\perp}\mathrm{e}^{-\mathrm{i}\omega t + \mathrm{i}n\phi} = \sum_{\sigma}\int \mathrm{d}\Gamma \frac{1}{2} M v_{\perp}^2 f_{\mathrm{L}}^1, \tag{7}$$

Here, Γ denotes the particle velocity space and M the particle mass. $v_{\parallel}$ and $v_{\perp}$ denote the parallel and perpendicular velocities of the particle guiding center drift motion, respectively. The sign σ represents particle species (electrons, ions and energetic particles). The perturbed distribution function f_{L}^1, defined in the Lagrangian frame, satisfies the following equation,

$$\frac{\mathrm{d}f_L^1}{\mathrm{d}t} = f_{\varepsilon}^0\frac{\partial H^1}{\partial t} - f_{P_\phi}^0\frac{\partial H^1}{\partial\varphi} - \nu_{\mathrm{eff}} f_{\mathrm{L}}^1, \tag{8}$$

where $f^0(\varepsilon, \psi)$ is the equilibrium distribution function of particles, assumed to be Maxwellian for thermal ions and electrons, and slowing down distribution for energetic ions. f_{ε}^0 and $f_{P_\phi}^0$ denote the derivatives with respect to the particle energy and canonical momentum, respectively. ψ is the poloidal magnetic flux. $\varepsilon = Mv^2/2 + Ze\Phi$ is the particle total energy with Z being the charge number and Φ being the equilibrium electrostatic potential. The total canonical momentum is defined as $P_\phi = MR^2\phi + Ze\psi$. ν_{eff} is the collision coefficient. The variable $H^1 = -\varepsilon_k H_{\mathrm{L}}\exp(-\mathrm{i}\omega t + \mathrm{i}n\phi)$ represents particle Lagrangian perturbation with $H_{\mathrm{L}} = [Mv_{\parallel}^2\vec{\kappa} \bullet \vec{\xi}_{\perp} + \mu(Q_{L\parallel} + \nabla B \bullet \vec{\xi}_{\perp})]/\varepsilon_k$. $\vec{\kappa} = (\vec{b} \bullet \nabla)\vec{b}$ is the magnetic curvature and $\mu = Mv_{\perp}^2/2B$ is the magnetic moment of particle, $\varepsilon_k = Mv^2/2$ the particle's kinetic energy, and $Q_{L\parallel} = \vec{b} \bullet \nabla \times (\vec{\xi} \times \vec{B})$ the parallel component of the magnetic field. The solution of equation (8) has been discussed in detail in [5]. Equations (1)–(8) form a close system to study the fishbone modes. In this work, the above equations are solved in a PEST-like straight field line (SFL), toroidal coordinate system (s, χ, ϕ). Here, the first variable s represents the square root of the normalized poloidal magnetic flux, varying between 0 (magnetic axis) and 1 (plasma boundary). The second and the third variables,χ, ϕ, correspond to a generic poloidal angle and the geometrical toroidal angle, respectively.

An experimental equilibrium configuration of HL-2A, with neutral beam injection (NBI) heated plasma, is considered. The equilibrium obtained from the EFIT code, as well as the relevant kinetic profiles, are shown in figure 1. The main parameters are: the toroidal magnetic field $B = 1.3$ T, the major/minor radii $R = 1.65$ m/$a = 0.4$ m, the central electron density $n_{\mathrm{e}}(0) = 1.6 \times 10^{19}$ (m^{-3}), the electron temperature $T_{\mathrm{e}}(0) = 1.5$ (keV), the ion temperature $T_{\mathrm{i}}(0) = 1.5$ (keV), the temperature ratio of the hot to thermal ions $T_{\mathrm{h}}/T_{\mathrm{i}} = 30$, the density fraction of hot ions $n_{\mathrm{h}}/n_{\mathrm{i}} = 0.04$, the on-axis safety factor $q(0) = 0.9$ and the edge safety factor $q(a) = 4.08$. In order to avoid the stabilizing effect of the plasma flow on the fishbone instability, the plasma equilibrium is assumed to be static. The energy distribution of energetic ions is a slowing-down function, and the pitch angle distribution is specified by Gaussian functions [5]. In this work, the orbit width of EPs and the particle collision are neglected. The

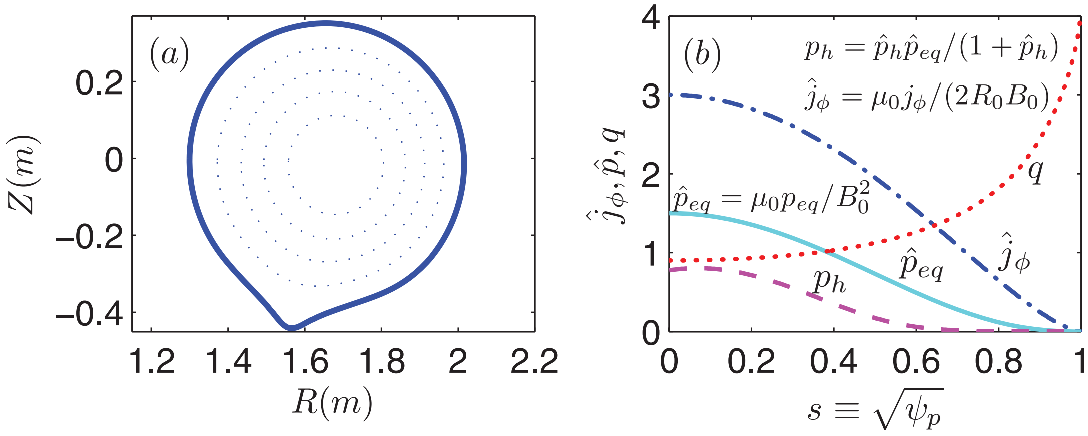

Figure 1. (*a*) The diverter configuration of HL-2A, and (*b*) the equilibrium kinetic profiles for the normalized current density $\widehat{j}_\phi = \mu_0 j_\phi/(2R_0B_0)$ (dash-dotted line), the equilibrium pressure $\widehat{p}_{eq} = \mu_0 p_{eq}/B_0^2$ (solid line), the pressure of energetic ions $p_h = \widehat{p}_h\widehat{p}_{eq}/(1+\widehat{p}_h)$ (dashed line) and the safety factor (dotted line), as functions of s, defined as the square root of the normalized poloidal magnetic flux.

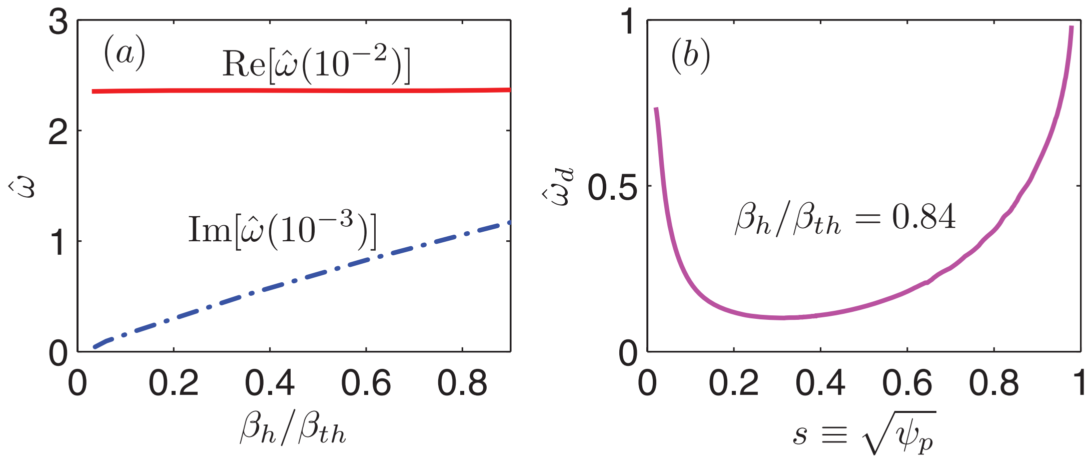

Figure 2. (*a*) Real (solid line) and imaginary (broken line) parts of the fishbone eigenvalue, normalized to the on-axis Alfvén frequency, i.e. $\widehat{\omega} = \omega/\omega_A(0)$, versus the beta fraction of energetic ions with beam energy $E_b = 45$ keV. (*b*) The normalized toroidal precessional drift frequency of energetic ions $\widehat{\omega}_d = \omega_{dh}/\omega_A(0)$, as a function of square root of the normalized poloidal magnetic flux.

contours in figure 1(*a*) are flux surfaces showing the diverter configuration of HL-2A, with the bold line representing the plasma boundary. The curves in figure 1(*b*) represent the normalized, flux surface averaged toroidal current density profile $\widehat{j}_\phi = \mu_0 j_\phi/(2R_0B_0)$ (dash-dotted line), the safety factor q (dotted line), the normalized plasma equilibrium pressure $\widehat{p}_{eq} = \mu_0 p_{eq}/B_0^2$ (solid line), and the pressure profile of energetic ions p_h (dashed line), as functions of s. The pressure of energetic ions was given by $p_h = \widehat{p}_h\widehat{p}_{eq}/(1+\widehat{p}_h)$ where the pressure fraction factor, for energetic ions, is defined as $\widehat{p}_h = p_h/p_{th}$. Here, p_{th} represents the pressure of thermal particles. The total pressure, which satisfies the equilibrium force balance, is the sum of the thermal and EPs pressures.

The diamagnetic drift of energetic particles is the dominant factor driving the fishbone instabilities. We shall only consider the mode resonance with toroidal precessional drift motion (including both the ∇B drift and the curvature drift) of EPs. The other resonances, due to bounce/transit motions of EPs, are neglected. With non-uniform radial distributions of density or temperature, energetic particles usually interact with the (stable) internal kink mode, driving the fishbone instability, as long as the EPs pressure is sufficiently large. Moreover, the real frequency of the fishbone mode is usually about half of the precessional drift frequency of EPs at the particle birth energy (i.e. $\omega_r \sim \omega_{dh}/2$). The growth rate of the mode is roughly a linear function of the EPs pressure [3]. Compared with previous studies based on the energy principle, the advantages of using the MARS-K code is the self-consistent treatment of not only the eigenvalue but also the mode eigenfunction for fishbone.

The MARS-K computed eigenvalues of the fishbone mode, for our equilibrium, are shown in figure 2(*a*), as function of β_h/β_{th}. The real and imaginary parts of the eigenvalues represent the real frequency (solid line) and the growth rate (broken line), respectively, of the fishbone mode. These quantities are normalized to the on-axis Alfvén frequency. Shown in figure 2(*b*) is the toroidal precessional drift frequency $\widehat{\omega}_d$, averaged over the particle velocity space and normalized to the on-axis Alfvén frequency, versus the plasma

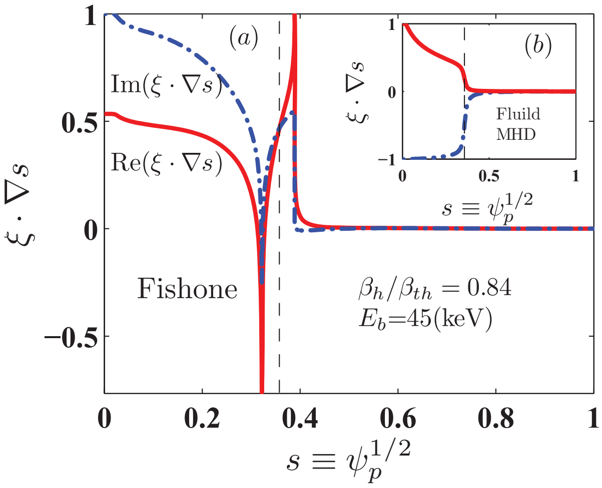

Figure 3. Real (solid lines) and imaginary parts (broken lines) of the normalized radial displacement of the plasma versus the minor radius, for (*a*) the fishbone mode, and (*b*) the single fluid MHD predicted ideal internal kink mode. The eigenfunctions are self-consistently computed with MARS-K. The vertical dashed line indicates the location of the $q = 1$ rational surface.

minor radius, at $\beta_\mathrm{h}/\beta_\mathrm{th} = 0.84$ and beam energy $E_\mathrm{b} = 45$ keV, based on the equilibrium from figure 1. The minimum value of the toroidal precession frequency of EPs is about 0.1 in our case. Figure 2(*a*) shows that the fishbone is excited by energetic ions, when $\beta_\mathrm{h}/\beta_\mathrm{th}$ is larger than a critical value of 0.03. The real frequency of the excited mode stays nearly constant, being in the same order of magnitude as compared to the toroidal precessional drift frequency, agreeing with theoretical expectations [3, 4]. In MARS-K, the toroidal precession frequency is calculated as $\omega_\mathrm{dh} = \partial J_\parallel/\partial s/\partial J_\parallel/\partial \varepsilon$, where $J_\parallel = \int v_\parallel \mathrm{d}l$ denotes the longitudinal adiabatic invariant of the particle motion. In the large aspect ratio approximation, the above expression for the precession frequency is roughly reduced to $\omega_\mathrm{dh} \propto q/r$. With a parabolic-like safety factor profile in the HL-2A plasma, the toroidal precession frequency is thus expected to decrease with s near the magnetic axis, and increase with s in the outer region. This is exactly what we numerically find, as shown in figure 2(*b*).

Figure 3 shows the MARS-K computed eigenmode structure, in terms of the (normalized) radial displacement of the plasma, for the $n = 1$, $m = 1$ harmonic, versus the plasma minor radius. Compared are displacements between (*a*) the fishbone mode and (*b*) an unstable ideal internal kink mode within the single fluid approximation. It is important to note that these eigenfunctions are obtained from self-consistent MARS-K computations. The fishbone mode is computed at $\beta_\mathrm{h}/\beta_\mathrm{th} = 0.84$, beam energy $E_\mathrm{b} = 45$ (keV), and with an eigenvalue of $\widehat{\omega} = (2.36 \times 10^{-2},\ 1.1 \times 10^{-3})$. The plasma displacement associated with the ideal internal kink is, as expected, nearly constant inside the $q = 1$ surface, and monotonically decays to zero outside the rational surface. What is interesting, however, is the more complicated mode structure for the fishbone instability. Sharp variation of the $m = 1$ displacement across the $q = 1$ surface is observed, with strong peaking occuring at the radial locations of $s_1 = 0.354$ and $s_2 = 0.389$.

This new feature of the fishbone mode structure results from the kinetic effects of energetic particles on the mode, as well as from the resonant interaction between the mode and the shear Alfvén waves, as will be elucidated next. We remark here that, in previous work, the eigenmode structure of fishbone is often assumed as a step-like function, making analytic utilization of the energy principal possible [3, 4]. What we find here shows that this may not always be a good approximation.

The resonance between the fishbone mode and the shear Alfvén waves occurs, when the real frequency of the fishbone, in the plasma frame, matches that of the Alfvén waves

$$\omega_\mathrm{r}^2 = \omega_\mathrm{A}^2(r) = (k_\parallel v_\mathrm{A})^2 = \left[\frac{nq(r) - m}{Rq(r)} v_\mathrm{A}\right]^2, \tag{9}$$

where v_A is the toroidal Alfvén speed defined at the magnetic axis. Note that, with relatively slow mode frequency (~the toroidal precession frequency of fast ions) for the fishbone, the above resonance can only occur near the $q = 1$ rational surface, where the parallel wave number $\kappa_\parallel$ is small. Thus, for an ordinary q-profile, there are two resonant positions, located from both sides of the $q = 1$ surface. The mode eigen-function is substantially modified near these two resonant surfaces, as shown in figure 3.

Even more interestingly, strong current sheets are formed at the radial locations of these two resonant surfaces, as shown in figure 4. These current sheets form part of the fishbone eigenfunction, as the self-consistent solution of the MHD-kinetic hybrid equations. For the case shown here, the perturbed parallel current density amplitude peaks at $q_1 = 0.97796$ and $q_2 = 1.02081$, corresponding to the radial positions of $s_1 = 0.354$ and $s_2 = 0.389$, respectively.

The radial gap between these two current sheets is numerically determined and shown in figure 5, as the distance between the upper and lower circles, at each computed mode frequency, which varies as a result of changing the temperature of EPs. The gap almost linearly increases with the mode frequency. On the other hand, the lines in figure 5 correspond to the analytic estimates following the exact solution of equation (9). Quantitative agreement between the numerical results and the analytic estimates confirm the shear Alfvén wave resonance nature for the fishbone mode. No sound wave resonance induced current sheets are observed in these computations, though theoretically such resonance, between the fishbone and the sound wave (or the slow magneto-acoustic wave) continuum, can also occur.

It is the conventional understanding that the EPs kinetic effects mainly act on the bulk part of the internal kink eigenmode (i.e. not inside the inertia layer which is normally very narrow). Toroidal computations allow us to investigate this aspect in more detail, also in the context of the mode coupling to the Alfvén waves as studied in this work. For this purpose, we apply an artificial window function along the plasma minor radius, of width $2\delta_s a$, as a multiplier to all the drift kinetic terms associated with the trapped EPs [16]. The function value is 0 inside the window and 1 outside the window. The window is symmetrically located from both sides of the $q = 1$ rational surface. By varying this numerical

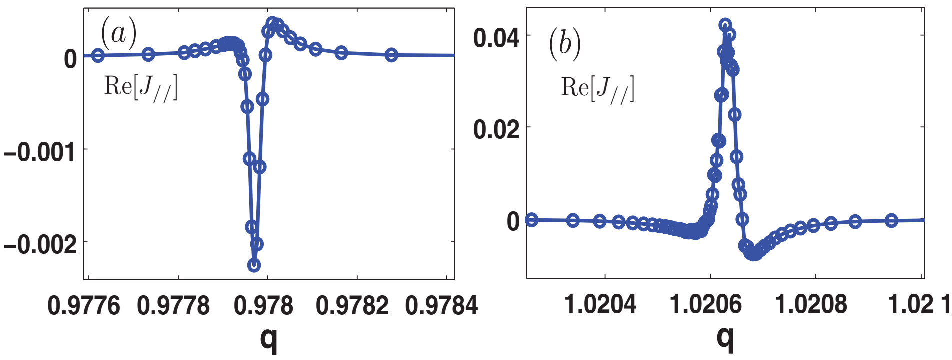

Figure 4. The self-consistently computed perturbed current sheets, located from both sides of the $q = 1$ rational surface, as a result of the wave-wave resonance between the fishbone mode and the shear Alfvén continuum. Plotted is the real part of the perturbed parallel current density versus the safety factor q, from the same MARS-K computation as in figure 3.

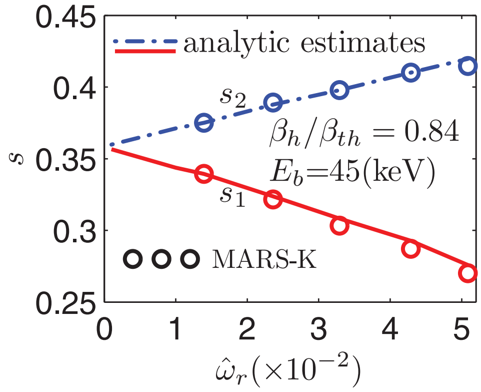

Figure 5. The radial positions of the resonant surfaces from both sides of the $q = 1$ rational surface, are plotted versus the real frequency $\widehat{\omega}_r = \omega_r/\omega_A(0)$ of the fishbone mode. The resonant surfaces occur due to interaction between the fishbone mode and the shear Alfvén waves.

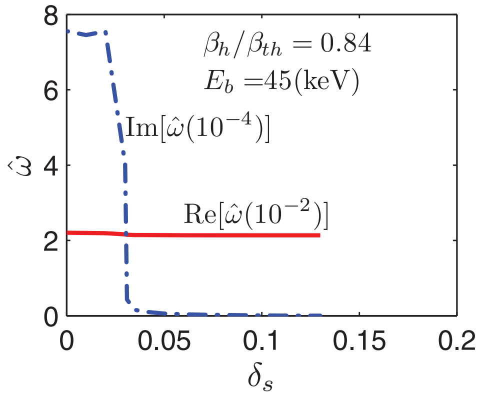

Figure 6. The real frequency (solid line) and growth rate (broken line) of the computed fishbone mode, as functions of δ_s, representing the width of the window for an artificial weighting function on the kinetic terms in the MARS-K model. The eigenvalue is normalized to the on-axis Alfvén frequency, $\widehat{\omega} = \omega/\omega_A(0)$.

parameter δ_s, we can study how the kinetic effects inside the layer affect the fishbone mode instability. The computational results, shown in figure 6, indicate that fishbone stability is not much affected, as long as the window width does not exceed the $q = 1$ inertia layer width, which is about $0.1a$ as shown in figure 3. On the other hand, a too large window, covering the whole inertia layer and beyond, quickly reduces the EPs drive, resulting in the loss of the fishbone excitation.

Figure 7 shows one example of the MARS-K computed fishbone eigenmode structure, but plotted in the 2D domain for the plasma core region. The same EPs parameters, as those in figure 3, are assumed. The $n = 1$, $m = 1$ internal kink structure is evident. Note, however, the sharp variations of the mode structure near the $q = 1$ rational surface, which is self-consistently generated due to the mode resonance with shear Alfvén waves. This is different from the conventional internal kink eigen-structure as predicted by the M3D code [12]. Finally, we remark that, as a linear eigenfunction, the toroidal phase of the computed plasma displacement is undetermined. Therefore, only the relative phase between the real and imaginary parts, shown in figure 7, has physics significance.

In summary, the non-perturbative toroidal modeling, using the well benchmarked MARS-K code, allows us to numerically investigate the resonant interaction physics

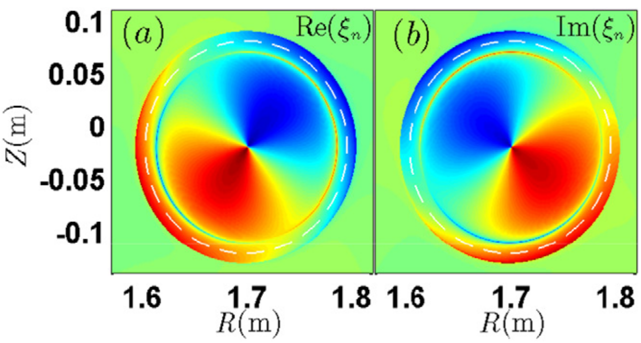

Figure 7. One example of the eigenmode structure of the $n = 1$ fishbone, computed with MARS-K and plotted on the poloidal plane for the core region of the plasma. Plotted are the real and imaginary parts of the plasma radial displacement. The dashed lines indicate the location of the $q = 1$ rational surface.

between the trapped EPs triggered fishbone mode and the shear Alfvén waves in tokamak plasmas. Such interaction is possible, thanks to the finite mode frequency driven by EPs toroidal precession, even in a static equilibrium. The Alfvén resonance qualitatively modifies the eigenmode structure of the fishbone, by introducing a double-peak structure in the perturbed parallel current density near the $q = 1$ rational surface, and by causing substantial plasma radial displacement reversal near the same surface. These new features should be taken into account in further development of more accurate fishbone models, as well as in the future interpretation of experimental results, provided that fine measurements can be made within the narrow inertial layer in experiments. Finally, this modification of the mode structure may have consequences for the local (particle, thermal, as well as momentum) transport across the inertial layer, as has previously been studied [17].

Acknowledgments

This work was supported by National Magnetic Confinement Fusion Science Program under grant Nos. 2013GB112009 and 2014GB124004, National Natural Science Foundation of China grant Nos 11175058 and 11428512. The work also partly received funding from the European Union's Horizon 2020 research and innovation programme under grant agreement number 633053 and from the RCUK Energy Programme (grant number EP/I501045). The views and opinions expressed herein do not necessarily reflect those of the European Commission.

References

[1] Bondeson A. *et al* 1994 *Phys. Rev. Lett.* **72** 2709
[2] Betti R. *et al* 1995 *Phys. Rev. Lett.* **74** 2949
[3] White R.B. *et al* 1985 *Phys. Fluids* **28** 278
[4] Zonca F. *et al* 2014 *Phys. Plasmas* **21** 072120
Zonca F. *et al* 2014 *Phys. Plasmas* **21** 072121
[5] Liu Y.Q. *et al* 2008 *Phys. Plasmas* **15** 112503
[6] Berkery J.W. *et al* 2014 *Phys. Plasmas* **21** 052505
[7] Wang Z. *et al* 2014 *Phys. Plasmas* **21** 042502
[8] Liu Y.Q. *et al* 2010 *Plasmas Phys. Control. Fusion* **52** 104002
[9] Menard J.E. *et al* 2014 *Phys. Rev. Lett.* **113** 255002
[10] Wang Z.R. *et al* 2015 *Phys. Rev. Lett.* **114** 145005
[11] Liu Y.Q. *et al* 2009 *Nucl. Fusion* **49** 035004
[12] Fu G.Y. *et al* 2006 *Phys. Plasmas* **13** 052517
[13] Shen W. *et al* 2015 *Phys. Plasmas* **22** 042510
[14] Vlad G. *et al* 2004 *Plasmas Phys. Control. Fusion* **46** S81
[15] Cole M. *et al* 2014 *Phys. Plasmas* **21** 072123
[16] Liu Y.Q. *et al* 2014 *Phys. Plasmas* **21** 056105
[17] Kolesnichenko Ya.I. *et al* 2010 *Nucl. Fusion* **50** 084017